Check for updates

Operational modal analysis of a rotating structure subject to random excitation using a tracking continuously scanning laser Doppler vibrometer via an improved demodulation method

L.F. Lyu and W.D. Zhu*

Department of Mechanical Engineering
University of Maryland, Baltimore County
1000 Hilltop Circle
Baltimore, MD 21250

Abstract

A new operational modal analysis (OMA) method is developed for estimation of modal parameters (MPs) of a rotating structure (RS) subject to random excitation using a nonuniform rotating beam model, an image processing method, and an improved demodulation method. The solution to the governing equation of a nonuniform rotating beam is derived, which can be considered as the response of the beam measured by a continuously scanning laser Doppler vibrometer (CSLDV) system. A recently developed tracking CSLDV system can track and scan the RS. The image processing method determines the angular position of the RS so that the tracking CSLDV system can sweep its laser spot along a time-varying path on it. The improved demodulation method obtains undamped mode shapes (UMSs) of the RS by multiplying its measured response by sinusoids whose frequencies are its damped natural frequencies (DNFs) that are obtained from the fast Fourier transform of the measured response. Experimental investigation of the OMA method

*Corresponding author. Tel: +1 410 455 3394; fax: +1 410 455 1052.

Email addresses: linfenl1@umbc.edu (L.F. Lyu), wzhu@umbc.edu (W.D. Zhu)

Zhu 1 VIB-21-1074

using the tracking CSLDV system is conducted, and MPs of a rotating fan blade (RFB), including DNFs and UMSs, with different constant speeds and its instantaneous MPs with a non-constant speed are estimated. Estimated first DNFs and UMSs of the stationary fan blade and RFB are compared with those from the lifting method that was previously developed by the authors.

Keywords: tracking continuously scanning laser Doppler vibrometer system; nonuniform rotating beam vibration theory; random excitation; improved demodulation method; operational modal analysis

1. Introduction

A laser Doppler vibrometer measures the velocity of a surface point on a structure along the direction of its laser beam [1, 2], which can be used to estimate modal parameters (MPs) of a linear structure. To provide high spatial resolution measurement, a scanning laser Doppler vibrometer (SLDV) system was developed that integrates computer-controlled orthogonal X- and Y- mirrors inside an optical head. The laser spot of the SLDV system is kept at a fixed position during one measurement and moved to another position for the next measurement. However, it can take a long time to obtain a full-field measurement of a structure using the SLDV system. A new continuous scanning laser Doppler vibrometer (CSLDV) system was proposed in Refs. [3-6] where a scanner with a set of orthogonal X- and Y- mirrors continuously sweeps the laser spot over a surface of a structure subject to sinusoidal excitation. Modal analysis methods were developed for a CSLDV system to estimate MPs of linear structures. Methods to estimate operational deflection shapes (ODSs) of a structure subject to sinusoidal excitation were developed in Refs. [7, 8] using a CSLDV system. One method is the demodulation method that can estimate ODSs of a structure by applying

Zhu 2 VIB-21-1074

Zhu

VIB-21-1074

a low-pass filter to the measured response multiplied by the sinusoids whose frequencies are the excitation frequency. The other method is the polynomial method that can estimate ODSs of the structure by processing the discrete Fourier transform of its measured response. The two methods were applied to measurements of structures subject to impact [9] and multi-sine [10] excitations. Chen et al. [11] developed a baseline-free method by combining the two methods to detect damage in beams subject to sinusoidal excitation. The demodulation method, which can only obtain ODSs of a structure subject to sinusoidal excitation, was subsequently used alone to detect damage in beams and plates [6, 12]. Xu et al. [13] introduced a free response shape of a structure to detect damage in it using the demodulation method. A modal estimation method based on a free response shape and the demodulation method was developed for a structure subject to impact excitation [14]. Yuan and Zhu [15] developed an extended demodulation method for estimation of MPs of a stationary structure subject to random excitation. Allen and Sracic [5] developed a lifting method to convert CSLDV measurement of a structure to measurements at virtual measurement points on it as if there were sensors there. Frequency response functions of the structure between its lifted measurements and an impact can be analyzed to estimate its MPs in the lifting method. Yang and Allen [16] developed an operational modal analysis (OMA) method using a CSLDV system for a structure subject to ambient excitation based on its harmonic transfer functions and harmonic power spectra [17]. An OMA method based on the harmonic transfer functions and lifting method was developed in Ref. [18] to simplify interpretation and processing of CSLDV measurement. In these two methods, estimated mode shapes (MSs) of a structure are represented by sums of harmonic functions that are spatially smooth. To describe MSs of the structure when there is a discontinuity on a scan path, a large number of harmonic functions are needed. Based on the lifting method, a

new OMA method was developed in Ref. [19] to estimate MPs of a beam and detect damage in it using a CSLDV system. This OMA method requires the CSLDV system to scan the structure with a high scan frequency to obtain its MPs, which is difficult to achieve when its natural frequencies are high.

To measure vibration of an RS, asynchronous point tracking [20] and synchronous point tracking [21-23] methods were developed to track a single point on it. Different methods were developed to extend point tracking to continuous scanning along lines or across areas on RSs [24-27]. Di Maio and Ewins [24] applied continuous tracking SLDV measurement methods to rotating bladed discs to estimate their ODSs. Gasparoni et al. [25] developed a method to track an RS and measure its ODSs by attaching an encoder to it. Martarelli et al. [26] developed a new method to track and estimate ODSs of RSs in coast-down tests, Khalil et al. [27] developed an experimental modal analysis method to measure MSs of an RFB whose angular position was tracked by an encoder attached to the fan shaft. Encoders are needed in these methods to obtain rotation speeds of these structures, and mirrors of tracking SLDV systems should be aligned with rotation axes of the structures to obtain accurate results [28-30]. However, it can be difficult to attach an encoder to a large RS such as a horizontal-axis wind turbine and align mirrors of a SLDV system with its rotation axis. Castellini and Tomasini [31] developed an image-based tracking laser vibrometer to measure the response of a single point on a moving windscreen wiper, but this method cannot estimate MSs or ODSs of an RS. A tracking CSLDV system and an OMA method based on an image processing method and the lifting method were developed in Ref. [32] to estimate MPs of a rotating fan blade (RFB). However, only the first MPs were estimated due to the limitation of the frame rate of the camera in the tracking CSLDV system and its scan frequency needs to be sufficiently high. A new Zhu VIB-21-1074

OMA method that can estimate higher MPs of an RS subject to random excitation, including damped natural frequencies (DNFs) and undamped mode shapes (UMSs), and has a low scan frequency to reduce the limitation of the camera's frame rate and measurement noise, is needed, which is studied here.

A new OMA method based on a nonuniform rotating beam model and an image processing method is developed for to estimation of MPs of an RS subject to random excitation, including DNFs and UMSs, using an improved demodulation method. A camera is integrated into a CSLDV system to track an RS by processing its images. The improved demodulation method can estimate UMSs of the RS by applying a low-pass filter to the measured response multiplied by sinusoids whose frequencies are its DNFs that are obtained from the fast Fourier transform (FFT) of the measured response. DNFs and UMSs of the RS with a constant speed and their instantaneous values in a short time duration for a non-constant speed can be estimated by the OMA method, which can be used to monitor vibration of a horizontal-axis wind turbine blade. One can subsequently use UMSs of the RS estimated by the OMA method to detect damage in it; this would be studied in some follow-up work, which has applications for wind turbine blade damage detection.

The tracking CSLDV system described in Ref. [32] was used to investigate the new OMA method by measuring the response of an RFB. The tracking CSLDV system consists of a laser vibrometer, a camera and a scanner. The fan whose one blade was scanned by the tracking CSLDV system was mounted to a stationary structure, which can be considered as a wind turbine model. Another fan was used to randomly excite the fan blade by its air flow. DNFs and UMSs of the RFB with constant and non-constant speeds were estimated, where NDFs and UMSs of the RFB with a non-constant speed were approximated by their instantaneous values in a short time duration. Zhu

Estimated first DNFs and UMSs of the stationary fan blade and RFB were compared with those estimated using the lifting method in Ref. [32]. Advantages and disadvantages of the demodulation and lifting methods in estimating MPs of an RS are discussed.

The remainder of the paper is structured as follows. A nonuniform rotating beam model that extends the uniform rotating beam model in Ref. [32] is presented in Sec. 2.1. The improved demodulation method for tracking CSLDV measurement of an RS is presented in Sec. 2.2. A method for processing tracking CSLDV mirror signals is described in Sec. 2.3. Experimental setup and results are presented in Secs. 3.1 and 3.2, respectively. Conclusions from this work are presented in Sec. 4.

2. Methodologies

2.1 Nonuniform Rotating Beam Model

An RFB can be considered as a nonuniform Euler-Bernoulli beam that rotates about the x-axis (Fig. 1). The length of the beam is d and it is attached to a rigid hub with a radius r. Let O-XYZ and o-xyz be an inertial and a rotating coordinate system, respectively. The origin o of o-xyz is at the rigid hub center, i.e., the rotation center. The origin O of O-XYZ is at corners of images captured by the camera of the tracking CSLDV system. Note that z- and Z-axes are parallel to each other.

By using the extended Hamilton's principle and neglecting transverse vibrations along x- and y-directions, the governing equation and associated boundary conditions (BCs) of the rotating beam in Fig. 1 excited by a distributed random force f(x,t) along the z-direction can be derived [33, 34]:

Zhu 6 VIB-21-1074

$$\rho(x)u_{tt}(x,t) + C[u_{t}(x,t)] + [EI(x)u_{xx}(x,t)]_{xx}$$

$$-u_{xx}(x,t)\dot{\theta}^{2}(t) \int_{x}^{r+d} \rho(\zeta)\zeta d\zeta + \rho(x)xu_{x}(x,t)\dot{\theta}^{2}(t) = f(x,t), \ r \leq x \leq r+d, \ t>0$$
(1)

$$|u(x,t)|_{x=r} = 0, |u_x(x,t)|_{x=r} = 0, |u_{xx}(x,t)|_{x=r+d} = 0, |EI(x)u_{xx}(x,t)|_{x}|_{x=r+d} = 0$$
 (2)

where x is the spatial position along the x-direction, t is time, $\theta(t)$ is the angular position of the rotating beam, u is the beam displacement along the z-direction at x and time t, a subscript and an overdot denote partial differentiation with respect to x and t, respectively, $\rho(x)$ is the mass per unit length of the rotating beam at x, x0 is the spatial damping operator, and x1 is the flexural rigidity of the beam at x2. Let x3 be a constant; Eq. (1) becomes

$$\rho(x)u_{tt}(x,t) + C[u_{t}(x,t)] + L[u(x,t)] = f(x,t), \ r \le x \le r + d, \ t > 0$$
(3)

where L is the spatial stiffness differential operator:

$$L[u] = \left[EI(x)u_{xx}(x,t) \right]_{xx} - u_{xx}(x,t)\Omega^{2} \int_{x}^{r+d} \rho(\zeta)\zeta \, d\zeta + \rho(x)xu_{x}(x,t)\Omega^{2},$$

$$r \le x \le r + d, \ t > 0$$
(4)

Note that rotation of the beam leads to the centrifugal stiffening term $-u_{xx}(x,t)\Omega^2 \int_x^{r+d} \rho(\zeta)\zeta d\zeta + \rho(x)xu_x(x,t)\Omega^2$ in Eq. (1). The solution to the equation of motion of the nonuniform rotating beam in Fig. 1 excited by a concentrated random force $f_a(t)$ at x_a can be derived in the Appendix:

$$u(x,t) = \sum_{i=1}^{\infty} \phi_i(x)\phi_i(x_a) \int_0^t f_a(t-\tau) \left(1/\omega_{d,i}\right) e^{-\zeta_i \omega_i \tau} \sin(\omega_{d,i}\tau) d\tau$$
 (5)

where $\phi_i(x)$ is the *i*-th MS of the corresponding undamped nonuniform rotating beam, and ω_i , ζ_i and $\omega_{d,i} = \omega_i \sqrt{1 - \zeta_i^2}$ are the *i*-th undamped natural frequency (UNF), modal damping ratio, and DNF of the beam, respectively.

Zhu 7 VIB-21-1074

2.2 Improved Demodulation Method

A time-varying scan path D(t) is generated on the RFB, and the tracking CSLDV system measures u by sweeping its laser spot along D(t). Discrete measurements of u are registered by the tracking CSLDV system with a sampling frequency F_{sa} . The measured response of the tracking CSLDV system can be expressed by Eq. (5) when only one concentrated force acts on the blade. Applying integration by part to Eq. (5) yields

$$u(x,t) = \sum_{i=1}^{\infty} \phi_i(x)\phi_i(x_a) \left\{ -\frac{e^{-\zeta\omega_i t} f_a(0)}{\omega_{d,i} \omega_i^2} \left[\zeta \omega_i \sin(\omega_{d,i} t) + \omega_{d,i} \cos(\omega_{d,i} t) \right] + \frac{f_a(t)}{\omega_i^2} + \int_0^t \frac{e^{-\zeta\omega_i t} f_a'(t-\tau)}{\omega_{d,i} \omega_i^2} \left[\zeta \omega_i \sin(\omega_{d,i} \tau) + \omega_{d,i} \cos(\omega_{d,i} \tau) \right] d\tau \right\}$$

$$(6)$$

Equation (6) can be written as

$$u(x,t) = \sum_{i=1}^{\infty} \phi_i(x)\phi_i(x_a) \left[A_i(t)\cos(\omega_{d,i}t) + B_i(t)\sin(\omega_{d,i}t) + C_i(t) \right]$$
(7)

where $A_i(t)$, $B_i(t)$ and $C_i(t)$ are functions related to the concentrated random force $f_a(t)$. Applying a bandpass filter with a passband containing only the i-th DNF of the RFB $\omega_{d,i}$ to the measured response in Eq. (7), one has

$$u_i(x,t) = \Phi_i(x)\cos(\omega_{d,i}t - \alpha) = \Phi_{I,i}(x)\cos(\omega_{d,i}t) + \Phi_{Q,i}(x)\sin(\omega_{d,i}t)$$
(8)

where $u_i(x,t)$ is the signal obtained after u(x,t) is band-pass filtered, $\Phi_i(x) = H_i \phi_i(x)$ in which H_i is a scalar factor, $\Phi_{I,i}(x) = \Phi_i(x) \cos(\omega_{d,i}t)$ and $\Phi_{Q,i}(x) = \Phi_i(x) \sin(\omega_{d,i}t)$ are in-plane and quadrature components of $\Phi_i(x)$, respectively, and α is a phase variable. Equation (8) is multiplied by $\cos(\omega_{d,i}t)$ and $\sin(\omega_{d,i}t)$ to obtain $\Phi_{I,i}(x)$ and $\Phi_{Q,i}(x)$, respectively:

$$u_{i}(x,t)\cos(\omega_{d,i}t) = \Phi_{I,i}(x)\cos^{2}(\omega_{d,i}t) + \Phi_{Q,i}(x)\sin(\omega_{d,i}t)\cos(\omega_{d,i}t)$$

$$= \frac{1}{2}\Phi_{I,i}(x) + \frac{1}{2}\Phi_{I,i}(x)\cos(2\omega_{d,i}t) + \frac{1}{2}\Phi_{Q,i}(x)\sin(2\omega_{d,i}t)$$
(9)

Zhu 8 VIB-21-1074

$$u_{i}(x,t)\sin(\omega_{d,i}t) = \Phi_{I,i}(x)\sin(\omega_{d,i}t)\cos(\omega_{d,i}t) + \Phi_{Q,i}(x)\sin^{2}(\omega_{d,i}t)$$

$$= \frac{1}{2}\Phi_{Q,i}(x) + \frac{1}{2}\Phi_{I,i}(x)\sin(2\omega_{d,i}t) - \frac{1}{2}\Phi_{Q,i}(x)\cos(2\omega_{d,i}t)$$
(10)

By applying a low-pass filter to $u_i(x,t)\cos(\omega_{d,i}t)$ and $u_i(x,t)\sin(\omega_{d,i}t)$, $\frac{1}{2}\Phi_{I,i}(x)\cos(2\omega_{d,i}t)$, $\frac{1}{2}\Phi_{I,i}(x)\sin(2\omega_{d,i}t)$ and $-\frac{1}{2}\Phi_{Q,i}(x)\cos(2\omega_{d,i}t)$ in Eqs. (9) and (10) can be eliminated so that $\Phi_{I,i}(x)$ and $\Phi_{Q,i}(x)$ can be obtained. When $\Phi_{I,i}(x)$ and $\Phi_{Q,i}(x)$ are obtained, $\Phi_{I}(x)$ can be determined using the relation in Eq. (9), and the i-th normalized MS of the undamped RFB can be estimated by dividing $\Phi_i(x)$ by its maximum value.

2.3 Method for Processing Mirror Signals of the tracking CSLDV System

Assume that the scan path D(t) is a straight line. When a stationary structure is scanned by a CSLDV system, the position of a laser spot on D(t) and the mirror rotation angle of the scanner in the CSLDV system have a linear relationship. The X-mirror feedback signal can describe the laser spot position (Fig. 2(a)). However, positions of the laser spot are not linearly related to feedback signals of X- and Y-mirrors in Fig. 2(b) when an RS is scanned by the tracking CSLDV system; hence, these mirror signals cannot describe the laser spot position. To obtain MSs of the RS with a constant speed, one needs mirror signals that are similar to the one shown in Fig. 2(a) to describe the laser spot position. A method is developed to describe the laser spot position by combining X- and Y-mirror signals. One attaches a mark to the RS to determine its angular position and generate a scan path on it. Position vectors of the mark $\mathbf{M}(t)$ and laser spot $\mathbf{P}(t)$ are

$$\mathbf{M}(t) = \left(a_m(t) - a_0, \ b_m(t) - b_0\right)^T = \left(d_m \cos(\Omega t), \ d_m \sin(\Omega t)\right)^T \tag{11}$$

$$\mathbf{P}(t) = \left(a_s(t) - a_0, b_s(t) - b_0\right)^T = \left(d_s(t)\cos(\Omega t), d_s(t)\sin(\Omega t)\right)^T \tag{12}$$

where (a_0, b_0) is the rotation center position, $(a_m(t), b_m(t))$ is the mark position, $(a_s(t), b_s(t))$

Zhu 9 VIB-21-1074

is the laser spot position, d_m and $d_s(t)$ are distances between the mark and rotation center and between the laser spot and rotation center at time t, respectively, as shown in Fig. 1, and the superscript T denotes transpose of a matrix. Note that $d_s(t)$ describes the position of the laser spot on D(t). Let $\mathbf{M}(t_1)$ and $\mathbf{M}(t_2)$ be position vectors of the mark at $t = t_1$ and $t = t_2$, respectively; the angle γ between $\mathbf{M}(t_1)$ and $\mathbf{M}(t_2)$ can be obtained by

$$\gamma = \operatorname{acos}\left(\frac{\mathbf{M}(t_1) \cdot \mathbf{M}(t_2)}{|\mathbf{M}(t_1)| \cdot |\mathbf{M}(t_2)|}\right)$$
(13)

Therefore, the speed of the RS R in revolutions per minute (rpm) can be written as

$$R = \frac{30\gamma}{\pi(t_2 - t_1)} \tag{14}$$

The adjusted mark position vector is

$$\mathbf{M}^{a} = ((a_{m} - a_{0})\cos(\beta) + (b_{m} - b_{0})\sin(\beta), (a_{m} - a_{0})\sin(\beta) + (b_{m} - b_{0})\cos(\beta))^{T}$$
 (15)

where β is a phase variable that adjusts the mark position. Different mark positions are obtained by changing β so that different scan paths D(t) can be generated on the RS. Positions of two end points of D(t) are

$$\begin{cases}
(a_1, b_1) = (a_0 + e_1 M_x, b_0 + e_1 M_y), C_1 > 1 \\
(a_2, b_2) = (a_0 + e_2 M_x, b_0 + e_2 M_y), 0 < C_2 < 1
\end{cases}$$
(16)

where e_1 and e_2 are two coefficients that can change the end point positions and the length of D(t), M_x is the X-component of \mathbf{M}^a , and M_y is the Y-component of \mathbf{M}^a . The laser spot is swept between the two end points when the CSLDV system tracks the RS. According to Eq. (12), the distance between the laser spot and rotation center is

Zhu 10 VIB-21-1074

VIB-21-1074

$$d_s(t) = |\mathbf{P}(t)| = \sqrt{(a_s(t) - a_0)^2 + (b_s(t) - b_0)^2}$$
(17)

Note that X- and Y-mirror signals obtained in experiment are used as $a_s(t)$ and $b_s(t)$, respectively, and one can obtain the laser spot position by using Eq. (17). The processed mirror signal using Eq. (17) is shown in Fig. 2(c), where two dashed lines at $t = t_s$ and $t = t_e$ indicate time instants when the laser spot reaches the two end points of the scan path, respectively. Mirror signals and the measured response between $t = t_s$ and $t = t_e$ can be used to obtain a UMS of the RS. The scan frequency of the tracking CSLDV system is $F_{\infty} = 0.5/(t_e - t_s)$. Therefore, the duration of the time interval (t_s, t_e) is short when F_{∞} is high. Since the improved demodulation method can be applied to a measured response in a short time duration, the OMA method can also estimate instantaneous DNFs and UMSs of an RS with a prescribed time-varying speed in the short time duration, since the speed of the RS $\hat{\theta}(t)$ can be regarded as a constant and there are no other time-dependent coefficients in Eq. (1).

3. Experimental Investigation

3.1 Experimental Setup

Zhu

The tracking CSLDV system with a Polytec OFV-533 laser Doppler vibrometer, a Basler camera, and a Cambridge 6240H scanner was used to track and scan an RFB whose rotating diameter is 139 mm (Fig. 3(a)). A more detailed description of the tracking CSLDV system and experimental setup was presented in Ref. [32]. An NI 9149 controller was used to control the scanner to sweep the laser spot of the vibrometer on the RFB. The vibrometer, scanner and camera were mounted on a tripod in Fig. 3(a) whose height was 141.1 cm. The camera whose frame rate was 25 frames per second captured rotating fan images. A black circular mark attached to the RFB, as shown

11

in Fig. 3(b), was used to determine its position. Images captured by the camera were converted to grayscale images and processed by IMAQ Vision within LabView to determine the real-time mark position, and the RFB position was determined when the mark position was determined. When the camera continuously captured rotating fan images, the tracking CSLDV system could track and scan the RFB (Fig. 4(a)). Feedback signals of X- and Y-mirrors of the scanner could describe X- and Y-mirror rotation angles that were considered to be linearly related to laser spot positions along X- and Y-directions. The maximum rotation speed that the tracking CSLDV system could track was about 30 rpm, which is higher than the rotation speed of a large rotating horizontal wind turbine that is about 5-15 rpm [35].

Random excitation applied on the RFB was provided by a small excitation fan whose radius was 15.24 cm (Fig. 4(b)). The rotating fan was mounted to a stationary aluminum structure. To facilitate image processing, the stationary structure and the wall behind it were covered with black cloth. The RFB that was scanned by the tracking CSLDV system was covered with a strip of reflective tape to enhance laser measurement. The fan center had a height of 122.3 cm. The distance between the fan to be scanned and the tracking CSLDV system was 174.6 cm. The distance between the fan to be scanned and excitation fan was 94.6 cm. To let the fan to be scanned rotate with different constant speeds, a voltage controller was connected to it, as shown in Fig. 4(b). The scan path in Fig. 4(a) ranged from $x_d / S = 0$ to $x_d / S = 1$, where x_d is the distance between the end point of the scan path near the rotation center and the laser spot, and S is the length of the scan path.

3.2 OMA results and discussion

The measured response of the RFB and X- and Y- mirror feedback signals are shown in Fig. 5(a) and (b), respectively, with F_{sa} =2500 Hz , F_{sc} = 0.125 Hz and R = 15.41 rpm . Note that Zhu 12 VIB-21-1074

 $F_{sc} = 1 \text{ Hz}$ when the speed of the RFB is non-constant, which means that $t_e - t_s = 0.5 \text{ s}$ in Sec. 2.3. Therefore, DNFs and UMSs of the RFB with a nonconstant speed were obtained in a short time duration of 0.5 s based on Sec. 2.3. Data of mirror signals were divided by their maximum values to normalize them. The processed mirror signal in Fig. 5(c) that was used to represent x_d/S was obtained by the method in Sec. 2.3. Three constant rotation speeds R = 9.79 rpm, 15.41 rpm and 24.28 rpm were prescribed by the voltage controller for the fan. Note that the RFB that was scanned by the tracking CSLDV system was a little more massive than the other two fan blades, since this fan blade was covered with a reflective tape. The fan was released from rest with an initial speed and started to rotate under the gravity effect; the tracking CSLDV system could track and scan the RFB with a non-constant speed. The speed of the RFB was determined by processing mark positions in images captured by the camera using Eqs. (11) and (12). Mark positions obtained with different constant rotation speeds and the non-constant rotation speed are shown in Figs. 6(a), (b), (c) and (d). Fan rotation speeds obtained from mark positions in Figs. 6(a), (b), (c) and (d) are shown in Fig. 6(e). Speeds of the RFB measured by the tracking CSLDV system with prescribed constant speeds slightly vary with time around its prescribed constant values.

The demodulation method in Sec. 2.2 was applied to the response measured in tests with different rotation speeds and processed mirror signals such as the one shown in Fig. 5(c). Minimum values of the processed mirror signal mean that the laser spot of the tracking CSLDV system reaches the end point $x_d / S = 0$ of the scan path and its maximum values mean that the laser spot of the tracking CSLDV system reaches the end point $x_d / S = 1$ of the scan path. The response in this time interval was measured by the tracking CSLDV system from one end point to the other one since mirror signals and the measured response were simultaneously recorded by the tracking Zhu

CSLDV system. A UMS of the RFB was obtained from the measured response in the time interval between neighboring minimum and maximum values of the processed mirror signal.

The procedure for obtaining the second UMS of the RFB with R = 15.41 rpm is described here as an example. The FFT of the measured response with R = 15.41 rpm is shown in Fig. 7(a), where two dashed lines at 27 and 28 Hz indicate the passband of the bandpass filter applied to the measured response and the dashed line at 27.64 Hz indicates the second DNF of the RFB with the constant speed R = 15.41 rpm. Note that the frequency of pseudo vibration caused by misalignment between mirrors of the tracking CSLDV system and the rotation axis of the fan is the rotation frequency of the fan blade, which is about 0.33-0.5 Hz when the rotation speed of the fan blade is 10-20 rpm. The spectral component in the measured response that corresponds to pseudo vibration can be filtered out by the passband filter since DNFs of the RFB are much higher than its rotation frequency. One can see that there are some other peaks near the one at 27.64 Hz in Fig. 7(a), where the one at 30 Hz corresponds to the second DNFs of the two other blades of the fan and the one near 25 Hz corresponds to the rotation frequency of the small excitation fan, whose excitation was transmitted to the fan blade via air flow. The measured rotation frequency of the small excitation fan was 26 Hz. The speed of airflow from the small excitation fan slightly decreased when it reached the fan that was scanned; so the measured frequency that corresponds to the rotation frequency was slightly lower than the measured rotation frequency of the small excitation fan. To determine if a DNF from the FFT of the measured response corresponds to the RFB that is scanned by the tracking CSLDV system, one can only excite the corresponding stationary fan blade and measure its response to estimate its corresponding DNF. The two measured DNFs would be close to each other since the rotation speed of the fan blade is small, and one can then be certain that the DNF from the FFT of Zhu 14 VIB-21-1074

the measured response corresponds to the fan blade scanned by the tracking CSLDV system. If the other peaks near the one at 27.64 Hz in Fig. 7(a) are very close to 27.64 Hz, one does not need to determine to which blade the peak at 27.64 Hz corresponds. The filtered measured response and processed mirror signal are shown in Fig. 7(b), where two dashed lines at $t = t_{s1}$ and $t = t_{e1}$ indicate the time interval selected to obtain the second UMS of the RFB. The FFT of the filtered measured response is shown in Fig. 7(c). The second normalized UMS of the RFB obtained from the filtered measured response and processed mirror signal in the time interval in Fig. 7(b) is shown in Fig. 7(d).

The first three estimated DNFs of the corresponding stationary fan blade in three tests under basically the same testing conditions are shown in Table 1, with their average values and standard derivations also shown there. The first three estimated normalized UMSs of the stationary fan blade in these tests are shown in Fig. 8(a), (b) and (c), respectively. Note that the fan blade was basically stationary, but slowly rotated when it was excited by air flow of the excitation fan. The first three DNFs of the RFB with three different constant speeds and a non-constant speed were also estimated, as shown in Table 2; its first three normalized UMSs are shown in Fig. 9(a), (b) and (c), respectively.

Estimated DNFs of the RFB in Table 2 increased with the constant speed of the RFB since there is a centrifugal stiffening term in Eq. (1), which is analytically shown here. Applying integration by parts and BCs in Eq. (2) yields

$$\int_{r}^{r+d} \phi_{i}(x) L \left[\phi_{j}(x) \right] dx = \int_{r}^{r+d} \phi_{i} \left\{ \left[EI(x) \phi_{j,xx} \right]_{xx} - \Omega^{2} \left[\phi_{j,xx} \int_{x}^{r+d} \rho(\zeta) \zeta \, d\zeta - 2\rho(x) x \phi_{j,x} \right] \right\} dx \\
= \int_{r}^{r+d} \left[EI(x) \phi_{i,xx} \phi_{j,xx} + \Omega^{2} \phi_{i,x} \phi_{j,x} \int_{x}^{r+d} \rho(\zeta) \zeta \, d\zeta \right] dx, \ r < x < r + d \tag{18}$$

Substituting Eq. (A.8) into Eq. (19) and setting i = j yield

Zhu 15 VIB-21-1074

$$\int_{r}^{r+d} \left[EI(x) \phi_{i,xx}^{2} + \Omega^{2} \phi_{i,x}^{2} \int_{x}^{r+d} \rho(\zeta) \zeta \, d\zeta \, \right] dx = \omega_{i}^{2}, \ r < x < r + d$$
 (19)

Since $r \le x \le r + d$, $\int_x^{r+d} \rho(\zeta) \zeta d\zeta \ge 0$, and the integral in Eq. (19) increases with Ω , which causes the natural frequency of the RFB ω_i to increase with its constant speed.

Estimated UMSs of the RFB are similar to those of a cantilever beam, as expected. Amplitudes of Estimated UMSs of the RFB have small amplitudes at $x_d / S = 0$, since the fan hub could have some vibration and the end point $x_d / S = 0$ of the scan path was not exactly at the end of the RFB that is connected to the fan hub. Some small differences among normalized UMSs of the stationary fan blade in Fig. 8 could be caused by errors in experiment and signal processing, e.g., tracking error caused by the fan blade slowly rotating, which could yield slight changes in scan paths in the three tests, and some error in the demodulation method. Scan paths might slightly differ when the CSLDV system tracked and scanned the RFB with different constant or non-constant speeds. Due to this reason, some error in the signal processing method, and the fact that the differential operator L changes with the speed of the RFB, there are some differences among estimated normalized UMSs of the RFB with different constant or non-constant speeds in Fig. 9. Note that a real wind turbine blade can have twisted blades and their vibration modes can include flap-wise bending modes, edge-wise bending modes, and torsional modes [36]. The current tracking CSLDV system can only estimate undamped flap-wise bending MSs of a rotating wind turbine blade; a two-dimensional scan scheme will be developed in the future to estimate undamped out-of-plane MSs of the whole surface of an RS, which can be used to estimate undamped torsional MSs of a rotating wind turbine blade. A 3D tracking SLDV system is required to estimate edge-wise MSs of a rotating wind turbine blade, which can be studied in the future.

The first DNFs and UMSs of the stationary fan blade and RFB with different constant speeds

Zhu 16 VIB-21-1074

estimated using the demodulation method and the lifting method in [32] are shown in Fig. 10, which are in excellent agreement. This validates OMAs by the demodulation and lifting methods. Note that the MPs of the RFB from the two methods were obtained from different measured responses with different scan frequecies when the fan blade rotated with the same speed, since the lifting method requires high scan frequency while the demodulation method does not. When the lifting method was used in Ref. [32], the Nyquist frequency of the tracking CSLDV system was limited by the camera's frame rate so that only the first mode of the RFB could be estimated there, but modes that the demodulation method could estimate did not depend on the frame rate of the camera in the tracking CSLDV system so that the demodulation method could estimate the first three modes of the RFB. On the other hand, the lifting method in Ref. [32] can estimate modal damping ratios and ODSs of an RS subject to random excitation, while the demodulation method cannot.

4. Conclusions

A new OMA method is developed for estimation of DNFs and UMSs of an RS with a constant speed and its instantaneous UMSs in a short time duration for a non-constant speed using a nonuniform rotating beam model, an image processing method, and an improved demodulation method. The improved demodulation method determines UMSs of the RS subject to random excitation by applying a low-pass filter to the measured response multiplied by sinusoids whose DNFs are estimated from the FFT of the measured response. The image processing method is used to track real-time positions of the RS so that the tracking CSLDV system can scan it. DNFs and UMSs of an RFB with a constant speed subject to random excitation and UMSs of the RFB with a non-constant speed in a short time duration were successfully estimated using the new method. Estimated DNFs of the RFB are theoretically and experimentally shown to increase with its constant Zhu VIB-21-1074

speed. The first estimated DNF and UMS of the stationary fan blade and RFB are compared with those from the lifting method in Ref. [32]. The demodulation method can estimate higher modes of an RS using a low frame-rate camera and a low scan frequency, while the lifting method cannot. The lifting method can estimate modal damping ratios and ODSs of an RS subject to random excitation, while the demodulation method cannot.

Acknowledgement

This work was supported by the National Science Foundation through Grant No. CMMI-1763024. The authors would like to thank D.-M. Chen and Y.F. Xu for valuable discussions on the tracking CSLDV system and demodulation method, respectively.

Appendix: Derivation of the Solution to the Equation of Motion of the Nonuniform Rotating Euler-Bernoulli Beam under a Concentrated Random Excitation Force

The eigenvalue problem of the corresponding undamped rotating beam can be written as

$$L[\phi] = \omega^2 \rho(x)\phi \tag{A.1}$$

where ω is its UNF, and ϕ is the corresponding MS that satisfies BCs in Eq. (2). Applying integration by parts and BCs in Eq. (2), one has

$$\int_{r}^{r+d} v(x) L[w(x)] dx
= \int_{r}^{r+d} v(x) \left\{ \left[EI(x) w_{xx}(x) \right]_{xx} - w_{xx}(x) \Omega^{2} \int_{x}^{r+d} \rho(\zeta) \zeta d\zeta + \rho(x) x w_{x}(x, t) \Omega^{2} \right\} dx
= \int_{r}^{r+d} \left[EI(x) w_{xx}(x) v_{xx}(x) + \Omega^{2} w_{x}(x) v_{x}(x) \int_{x}^{r+d} \rho(\zeta) \zeta d\zeta \right] dx
= \int_{r}^{r+d} w(x) L[v(x)] dx, \qquad r \le x \le r+d, \ t > 0$$
(A.2)

where v(x) and w(x) are two comparison functions that satisfy BCs for ϕ . Hence L is self-adjoint. Let v(x) = w(x) in Eq. (A.2); one has

Zhu 18 VIB-21-1074

$$\int_{r}^{r+d} w(x) L[w(x)] dx = \int_{r}^{r+d} [EI(x)w_{xx}^{2}(x) + \Omega^{2}w_{x}^{2}(x) \int_{x}^{r+d} \rho(\zeta)\zeta d\zeta] dx \ge 0,$$

$$r \le x \le r+d, \ t > 0$$
(A.3)

which means that L is positive definite. One also has

$$\int_{r}^{r+d} v(x)\rho(x)w(x)dx = \int_{r}^{r+d} w(x)\rho(x)v(x)dx, \ r \le x \le r+d, \ t > 0$$
(A.4)

$$\int_{r}^{r+d} w(x)\rho(x)w(x)dx = \int_{r}^{r+d} \rho(x)w^{2}(x)dx \ge 0, \ r \le x \le r+d, \ t > 0$$
 (A.5)

which mean that the spatial mass operator $\rho(x)$ is self-adjoint and positive definite. By the expansion theorem, the solution to Eq. (3) is [34]

$$u(x, t) = \sum_{i=1}^{\infty} \phi_i(x)q_i(t)$$
 (A.6)

where $q_i(t)$ is the *i*-th generalized coordinate. Since L and $\rho(x)$ are self-adjoint and positive definite, eigenfunctions of the corresponding undamped rotating beam are real and can be normalized to satisfy orthonormality relations

$$\int_{r}^{r+d} \phi_{i}(x) \rho(x) \phi_{j}(x) dx = \delta_{ij}$$
(A.7)

$$\int_{r}^{r+d} \phi_{i}(x) L\left[\phi_{j}(x)\right] dx = \omega_{i}^{2} \delta_{ij}$$
(A.8)

where δ_{ij} is Kronecker delta and ω_i is the i-th real UNF of the rotating beam. It is assumed that $C=k\,\rho(x)$, where k is a constant [34]. Substituting Eq. (A.6) into Eq. (3), multiplying the resulting equation by ϕ_j , integrating the resulting equation from x=r to x=r+d, and applying Eqs. (A.4) and (A.5) and the expression $\int_r^{r+d}\phi_i(x)C\left[\phi_j(x)\right]dx=k\delta_{ij}$ to the resulting equation yield

$$\ddot{q}_{i}(t) + k\dot{q}_{i}(t) + \omega_{i}^{2}q_{i}(t) = \int_{a}^{r+d} \phi_{i}(x)f(x,t)dx$$
 (A.9)

Zhu 19 VIB-21-1074

Considering modes of interest of the nonuniform rotating beam are underdamped, one has $k=2\zeta_i\omega_i$ for the modes with $0<\zeta_i<1$. When $0< k\leq 2\omega_i$, the modal damping ratios ζ_i satisfy $0<\zeta_i<1$. Let Eq. (1) have zero initial conditions; the solution to Eq. (A.9) is

$$q_i(t) = \int_0^t \int_r^{r+d} \phi_i(x) f(x, t - \tau) g_i(\tau) dx d\tau$$
(A.10)

where

$$g_i(t) = \left(1/\omega_{d,i}\right)e^{-\zeta_i\omega_i t}\sin(\omega_{d,i}t) \tag{A.11}$$

is the unit impulse response function that corresponds to the i-th mode of the nonuniform rotating beam. Substituting Eq. (A.11) into Eq. (A.6) yields

$$u(x,t) = \sum_{i=1}^{\infty} \phi_i(x) \int_0^t \int_r^{r+d} \phi_i(x) f(x,t-\tau) g_i(\tau) dx d\tau$$
 (A.12)

If a concentrated random force $f_a(t)$ is applied on the nonuniform rotating beam at x_a , one has

$$f(x,t) = \delta(x - x_a) f_a(t)$$
(A.13)

where δ is Dirac delta function. The solution to the equation of motion of the nonuniform rotating beam excited by a concentrated random force in Eq. (5) is obtained by substituting Eq. (A.13) into Eq. (A.12).

References

- [1] Bell, J.R., and Rothberg, S.J., 2000, "Laser Vibrometers and Contacting Transducers, Target Rotation and Six Degree-of-freedom Vibration: What Do We Really Measure?" Journal of Sound Vibration, 237, pp.245–261.
- [2] Rothberg, S., Allen, M., and Castellini, P., 2017, "An International Review of Laser Doppler Zhu 20 VIB-21-1074

- Vibrometry: Making Light Work of Vibration Measurement," Optics and Lasers in Engineering, 99(1), pp.11–22.
- [3] Sriram, P., Hanagud, S., Craig, J., and Komerath, N.M., 1990, "Scanning Laser Doppler Technique for Velocity Profile Sensing on a Moving Surface," Applied Optics, 29(16), pp.2409-2417.
- [4] Sriram, P., Hanagud, S., and Craig, J., 1992, "Mode Shape Measurement Using a Scanning Laser Doppler Vibrometer," The International Journal of Analytical and Experimental Modal Analysis, 7(3), pp. 169–178.
- [5] Allen, M.S., and Sracic, M.W., 2010, "A New Method for Processing Impact Excited Continuous-scan laser Doppler Vibrometer Measurements," Mechanical Systems and Signal Processing, 24(3), pp.721–735.
- [6] Chen, D.M., Xu, Y.F., and Zhu, W.D., 2016, "Damage Identification of Beams Using a Continuously Scanning laser Doppler Vibrometer System," Journal of Vibration and Acoustics, 138(5), 05011.
- [7] Stanbridge, A., and Ewins, D., 1996, "Using a Continuously-Scanning Laser Doppler Vibrometer for Modal Testing," 14th International Modal Analysis Conference (IMAC), Dearborn, MI, Feb. 12–15, pp. 816–822.
- [8] Stanbridge, A., and Ewins, D., 1999, "Modal Testing Using a Scanning Laser Doppler Vibrometer," Mechanical Systems and Signal Processing, 13(2), pp.255–270.
- [9] Stanbridge, A., Ewins, D., and Khan, A., 2000, "Modal Testing Using Impact Excitation and

Zhu 21 VIB-21-1074

- a Scanning LDV," Shock and Vibration, 7(2), pp.91–100.
- [10] Di Maio, D., and Ewins, D., 2011, "Continuous Scan, a Method for Performing Modal Testing
 Using Meaningful Measurement Parameters; Part I," Mechanical Systems and Signal
 Processing, 25(8), pp. 3027–3042.
- [11] Chen, D.M., Xu, Y.F., and Zhu, W.D., 2017, "Experimental Investigation of Notch-type Damage Identification with a Curvature-based Method by Using a Continuously Scanning Laser Doppler Vibrometer System," Journal of Nondestructive Evaluation, 36(2), p. 38.
- [12] Chen, D.M., Xu, Y.F., and Zhu, W.D., 2018, "Identification of Damage in Plates Using Full-field Measurement with a Continuously Scanning laser Doppler Vibrometer System, Journal of Sound and Vibration, 422, pp.542–567.
- [13] Xu, Y.F., Chen, D.M., and Zhu, W.D., 2017 Damage Identification of Beam Structures Using Free Response Shapes Obtained by Use of a Continuously Scanning laser Doppler Vibrometer System, Mechanical Systems and Signal Processing, 92, pp. 226–247.
- [14] Xu, Y.F., Chen, D.M., and Zhu, W.D., 2020, "Modal Parameter Estimation Using Free Response Measured by a Continuously Scanning Laser Doppler Vibrometer System with Application to Structural Damage Identification," Journal of Sound and Vibration, 485, 115536.
- [15] Yuan, K., and Zhu, W. D. 2021, "Estimation of Modal Parameters of a Beam under Random Excitation Using a Novel 3D Continuously Scanning Laser Doppler Vbrometer System And an Extended Demodulation Method." Mechanical Systems and Signal Processing, 155, 107606.

Zhu 22 VIB-21-1074

- [16] Yang, S., and Allen, M.S., 2012, "Output-only Modal Analysis Using Continuous-scan Laser Doppler Vibrometry and Application to a 20kw Wind Turbine, Mechanical Systems and Signal Processing, 31, pp.228–245.
- [17] Wereley, N.M., and Hall, S.R., 1990, "Frequency Response of Linear Time Periodic Systems," 29th IEEE Conference on Decision and Control, Honolulu, HI, USA, 6, pp.3650-3655.
- [18] Yang, S., and Allen, M.S., 2014, "Lifting Approach to Simplify Output-only Continuous-scan Laser Vibrometry," Mechanical Systems and Signal Processing, 45(2), pp.267–282.
- [19] Xu, Y.F., Chen, D.M., and Zhu, W.D., 2019, "Operational Modal Analysis Using Lifted Continuously Scanning Laser Doppler Vibrometer Measurements and Its Application to Baseline-free Structural Damage Identification," Journal of Vibration and Control, 25(7), pp.1341-1364.
- [20] Stanbridge, A. B., Martarelli, M., and Ewins, D. J., 2001, "Rotating disc vibration analysis with a circular-scanning LDV." in Proceedings of SPIE, the International Society for Optical Engineering, 4359, pp. 464-469.
- [21] Bucher, I., Schmiechen, P., Robb, D. A., and Ewins, D. J., 1994, "Laser-based Measurement System for Measuring the Vibration on Rotating Discs." in First International Conference on Vibration Measurements by Laser Techniques: Advances and Applications, 2358, pp. 398-408.
- [22] Castellini, P., Giovanucci, F., Nava-Mambretti, G., Scalise, L., and Tomasini, E. P., 1998,
 "Vibration Analysis of Tyre Treads: a In-plane Laser Vibrometry Approach." In Society for
 Experimental Mechanics, Inc, 16 th International Modal Analysis Conference. 2, pp. 1732Zhu

 23

 VIB-21-1074

1738.

- [23] Fioretti, A., Di Maio, D., Ewins, D. J., Castellini, P., and Tomasini, E. P., 2010, "Deflection Shape Reconstructions of a Rotating Five-blade Helicopter Rotor from TLDV Measurements." in AIP Conference Proceedings, 1253(1), pp. 17-28.
- [24] Di Maio, D., and Ewins, D. J., 2010, "Applications of Continuous Tracking SLDV Measurement Methods to Axially Symmetric Rotating Structures Using Different Excitation Methods." Mechanical Systems and Signal Processing, 24(8), pp. 3013-3036.
- [25] Gasparoni, A., Allen, M. S., Yang, S., Sracic, M. W., Castellini, P., and Tomasini, E. P., 2010, "Experimental Modal Analysis on a Rotating Fan Using Tracking-CSLDV." in AIP Conference Proceedings, 1253(1), pp. 3-16.
- [26] Martarelli, M., Castellini, P., Santolini, C., and Tomasini, E. P. 2011, "Laser Doppler Vibrometry on Rotating Structures in Coast-down: Resonance Frequencies and Operational Deflection Shape Characterization." Measurement Science and Technology, 22(11), 115106.
- [27] Khalil, H., Kim, D., Nam J., and Park, K., 2015, "Operational Deflection Shape of Rotating Object Using Tracking Laser Doppler Vibrometer," 2015 IEEE International Conference on Electronics, Circuits, and Systems, Cairo, pp.693-696.
- [28] Halkon, B. J., Frizzel, S. R., and Rothberg, S. J., 2003, "Vibration Measurements Using Continuous Scanning Laser Vibrometry: Velocity Sensitivity Model Experimental Validation." Measurement Science and Technology, 14(6), p. 773.
- [29] Halkon, B. J., and Rothberg, S. J., 2003, "Vibration Measurements Using Continuous

Zhu 24 VIB-21-1074

- Scanning Laser Doppler Vibrometry: Theoretical Velocity Sensitivity Analysis with Applications." Measurement science and technology, 14(3), p. 382.
- [30] Halkon, B. J., and Rothberg, S. J., 2006, "Vibration Measurements Using Continuous Scanning Laser Vibrometry: Advanced Aspects in Rotor Applications." Mechanical systems and signal processing, 20(6), pp. 1286-1299.
- [31] Castellini, P., and Tomasini, E. P., 2004, "Image-based tracking laser Doppler vibrometer." Review of scientific instruments, 75(1), pp. 222-232.
- [32] Lyu, L. F., and Zhu, W. D. 2021, "Operational Modal Analysis of a Rotating Structure under Ambient Excitation Using a Tracking Continuously Scanning Laser Doppler Vibrometer System." Mechanical Systems and Signal Processing, 152, 107367.
- [33] Zhu, W.D., and Mote, C.D., Jr. 1997, "Dynamic Modeling and Optimal Control of Rotating Euler-Bernoulli Beams," Journal of Dynamic Systems, Measurement, and Control, 119(4) pp.802–808.
- [34] Meirovitch, L., Analytical Methods in Vibrations, Macmillan Co, 1967.
- [35] Jonkman, J., Butterfield, S., Musial, W., and Scott, G., 2009, "Definition of a 5-MW Reference Wind Turbine for Offshore System Development," (No. NREL/TP-500-38060), National Renewable Energy Lab. (NREL), Golden, CO.
- [36] Acar, G. D., and Feeny, B. F., 2018, "Bend-bend-twist Vibrations of a Wind Turbine Blade." Wind Energy, 21(1), pp. 15-28.

Zhu 25 VIB-21-1074

Table caption list:

Table 1 DNFs of the stationary fan blade from three tests under basically the same testing conditions Table 2 DNFs of the RFB with different speeds



Table 1 DNFs of the stationary fan blade from three tests under basically the same testing conditions

Test number	First DNF (Hz)	Second DNF (Hz)	Third DNF (Hz)
1	6.227	27.197	54.36
2	6.233	27.23	54.25
3	6.224	27.19	54.30
Average value	6.228	27.206	54.303
Standard derivation	0.0037	0.0174	0.045

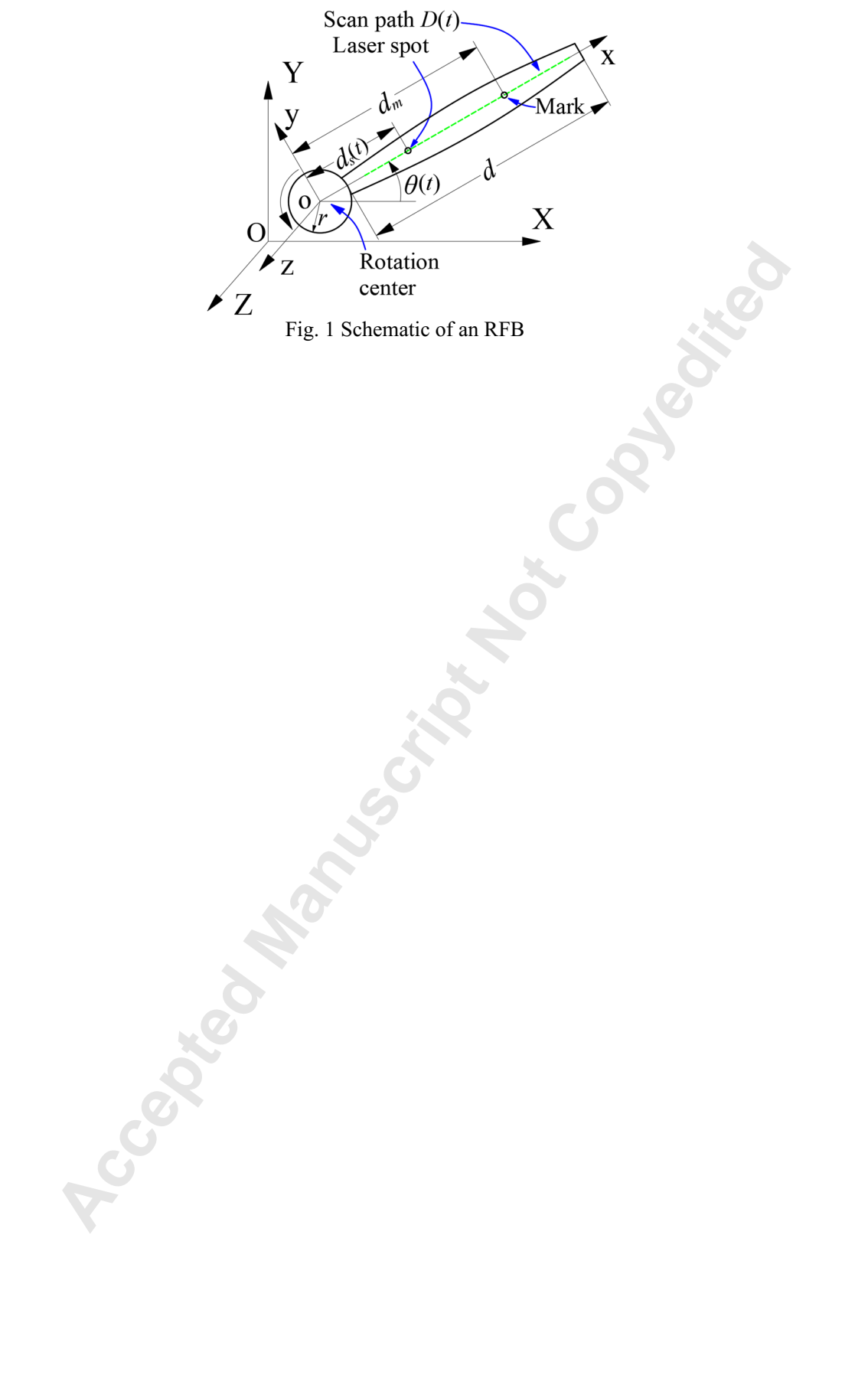
Table 2 DNFs of the RFB with different speeds

	First DNF (Hz)	Second DNF (Hz)	Third DNF (Hz)
9.79	6.375	27.33	54.79
15.41	6.56	27.64	56.37
24.28	6.75	27.85	57.16
Non-constant	6.27	27.41	55.02.

Figure caption list:

- Fig. 1 Schematic of an RFB
- Fig. 2 (a) Simulated X-mirror signal for scanning a stationary structure; (b) simulated X- and Y-mirror signals for scanning an RS; and (c) the processed mirror signal by combining X- and Y-mirror signals in (b) with a simulated measured response.
- Fig. 3 (a) Picture of the tracking CSLDV system for RS vibration measurement, and (b) a picture of the fan whose blade with a mark is tracked and scanned by the tracking CSLDV system.
- Fig. 4 (a) Schematic of RS vibration measurement using the tracking CSLDV system, and (b) the experimental setup for RS vibration measurement using the tracking CSLDV system.
- Fig. 5 (a) Measured response of the RFB under random excitation with R = 15.41 rpm, (b) the feedback signals of X- and Y-mirrors when R = 15.41 rpm, and (c) the processed mirror signal with R = 15.41 rpm.
- Fig. 6 (a) Measured mark position when R = 9.79 rpm, (b) the measured mark position when R = 15.41 rpm, (c) the measured mark position when R = 24.28 rpm, (d) the measured mark position with the non-constant rotation speed, and e) measured rotation speeds of the fan blade with the constant and non-constant rotation speeds based on the mark positions in (a), (b), (c) and (d).
- Fig. 7 (a) FFT of the measured response of the RFB under random excitation when R = 15.41 rpm, (b) the measured response in (a) that is filtered by a bandpass filter whose pass band is 27-28 Hz and processed mirror signal, (c) the FFT of the filtered measured response in (a), and (d) the second normalized UMS obtained from the filtered measured response and processed mirror signal in (b).
- Fig. 8 (a) First, (b) second and (c) third normalized UMSs of the stationary fan blade obtained in the three tests.
- Fig. 9 (a) First, (b) second and (c) third normalized UMSs of the RFB with different rotation speeds.
- Fig. 10 First UMSs and DNFs of (a) the stationary fan blade, (b) the RFB with R = 10.9 rpm, (c) the RFB with R = 16.04 rpm, and (d) the RFB with R = 24.12 rpm estimated using the demodulation method and the lifting method in Ref. [32].

Zhu 29 VIB-21-1074



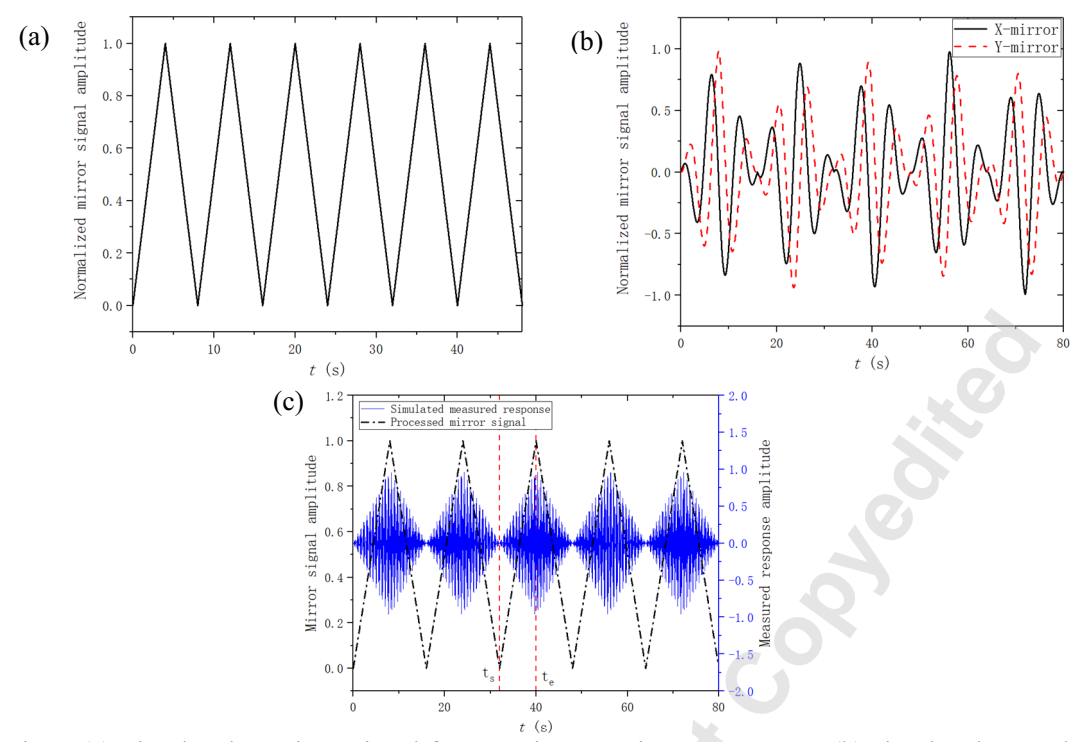
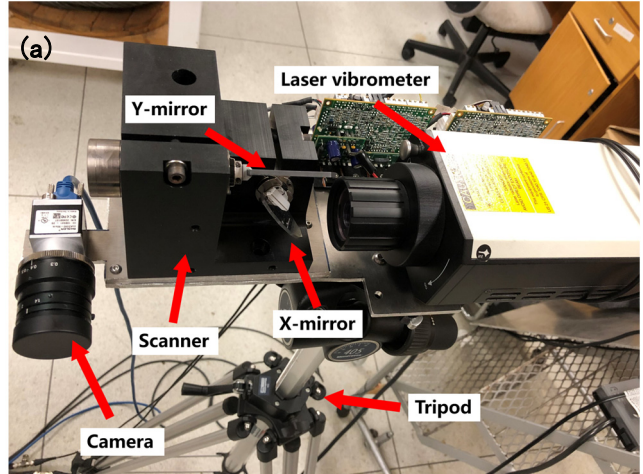


Fig. 2 (a) Simulated X-mirror signal for scanning a stationary structure; (b) simulated X- and Y-mirror signals for scanning an RS; and (c) the processed mirror signal by combining X- and Y-mirror signals in (b) with a simulated measured response.



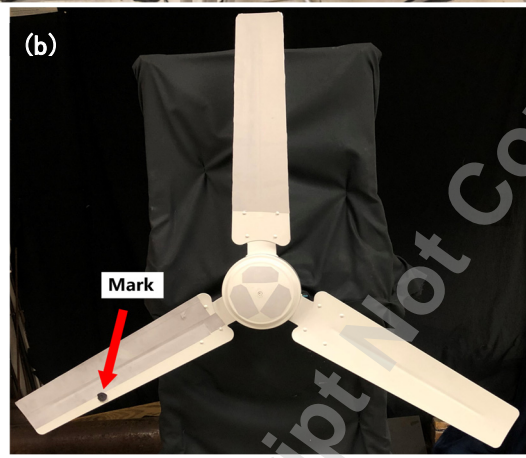


Fig. 3 (a) Picture of the tracking CSLDV system for RS vibration measurement, and (b) a picture of the fan whose blade with a mark is tracked and scanned by the tracking CSLDV system.

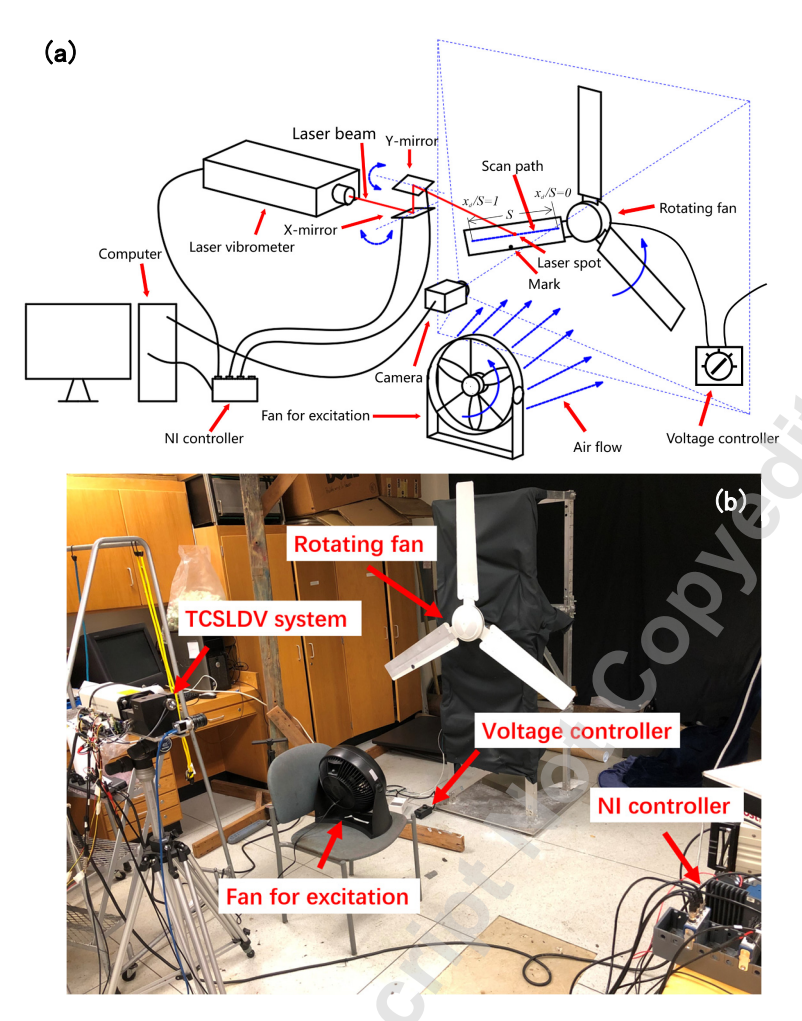


Fig. 4 (a) Schematic of RS vibration measurement using the tracking CSLDV system, and (b) the experimental setup for RS vibration measurement using the tracking CSLDV system.

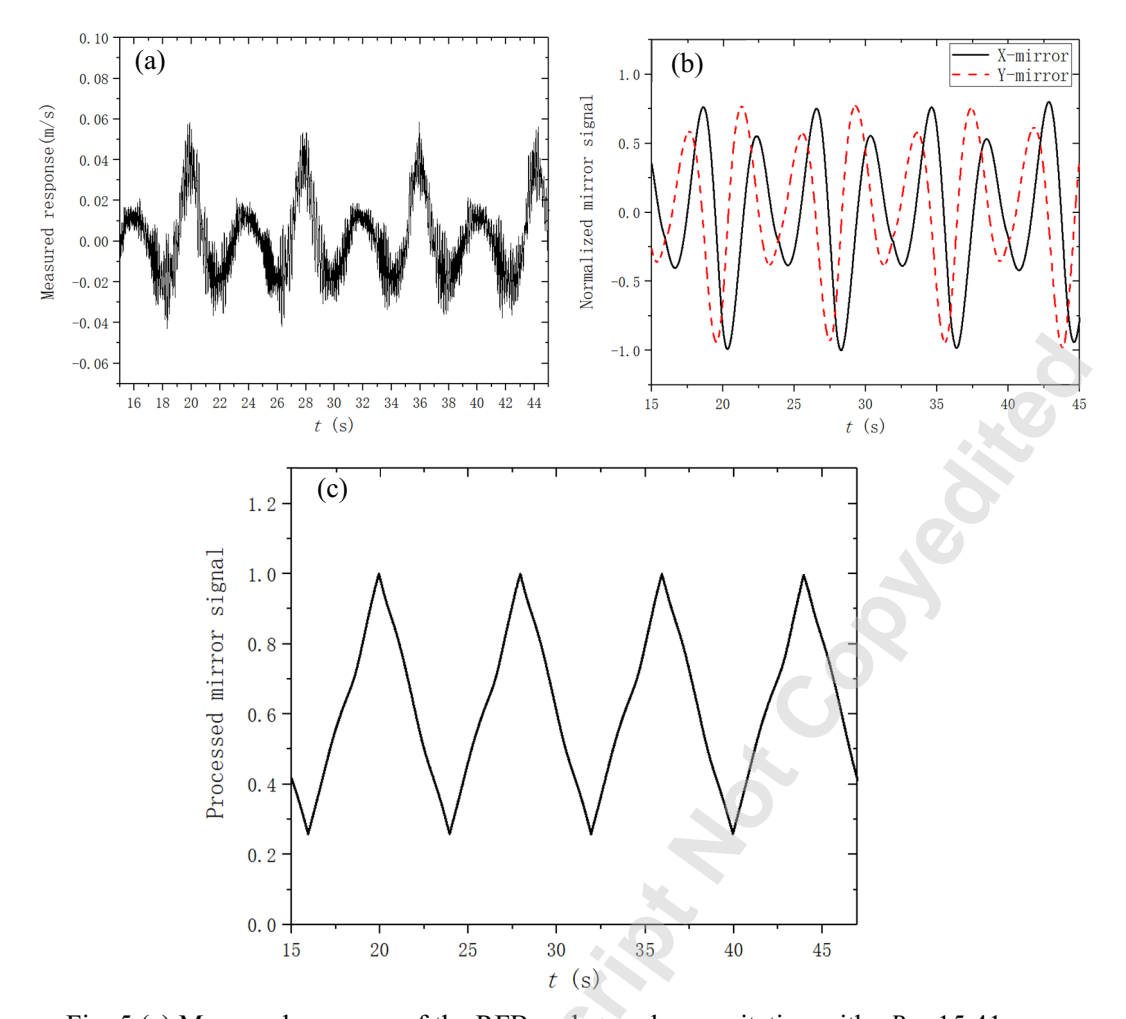


Fig. 5 (a) Measured response of the RFB under random excitation with $R=15.41~\rm rpm$, (b) the feedback signals of X- and Y-mirrors when $R=15.41~\rm rpm$, and (c) the processed mirror signal with $R=15.41~\rm rpm$.

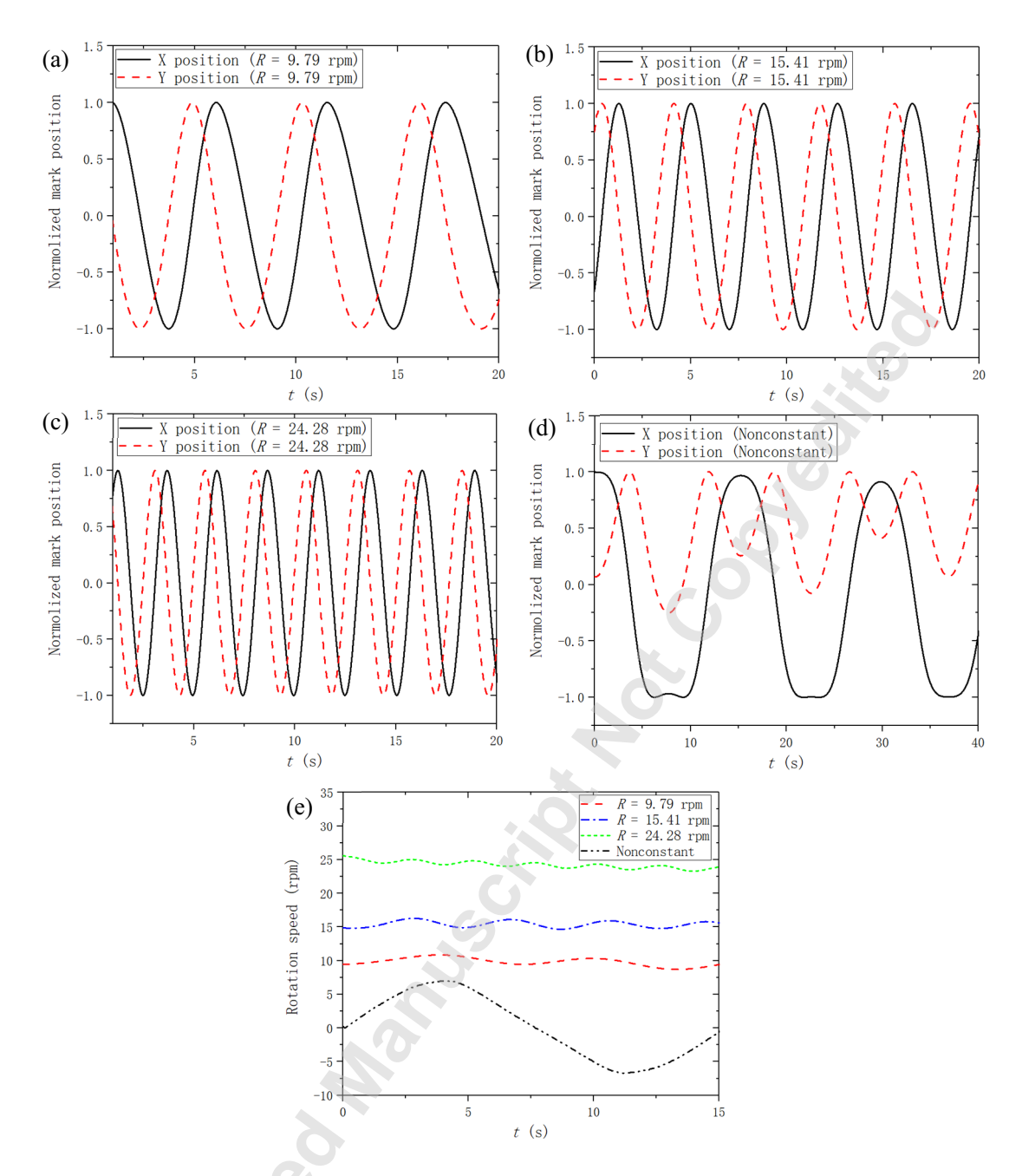


Fig. 6 (a) Measured mark position when R = 9.79 rpm, (b) the measured mark position when R = 15.41 rpm, (c) the measured mark position when R = 24.28 rpm, (d) the measured mark position with the non-constant rotation speed, and e) measured rotation speeds of the fan blade with the constant and non-constant rotation speeds based on the mark positions in (a), (b), (c) and (d).

Zhu 35 VIB-21-1074

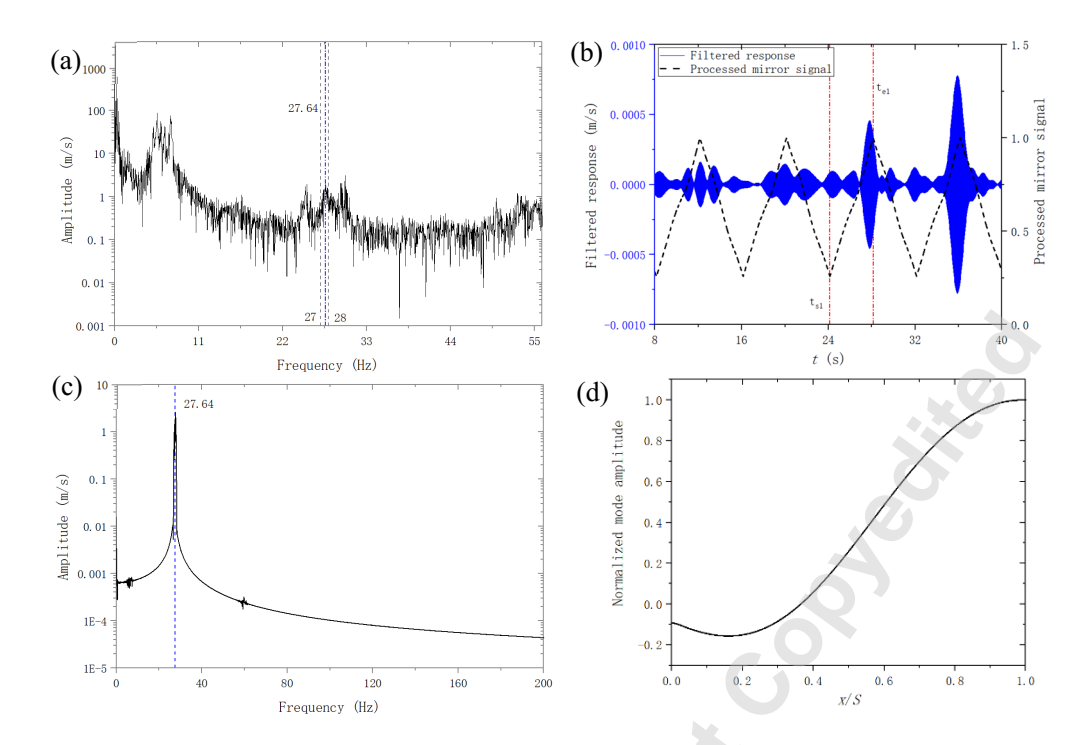


Fig. 7 (a) FFT of the measured response of the RFB under random excitation when R = 15.41 rpm, (b) the measured response in (a) that is filtered by a bandpass filter whose pass band is 27-28 Hz and processed mirror signal, (c) the FFT of the filtered measured response in (a), and (d) the second normalized UMS obtained from the filtered measured response and processed mirror signal in (b).

Zhu 36 VIB-21-1074

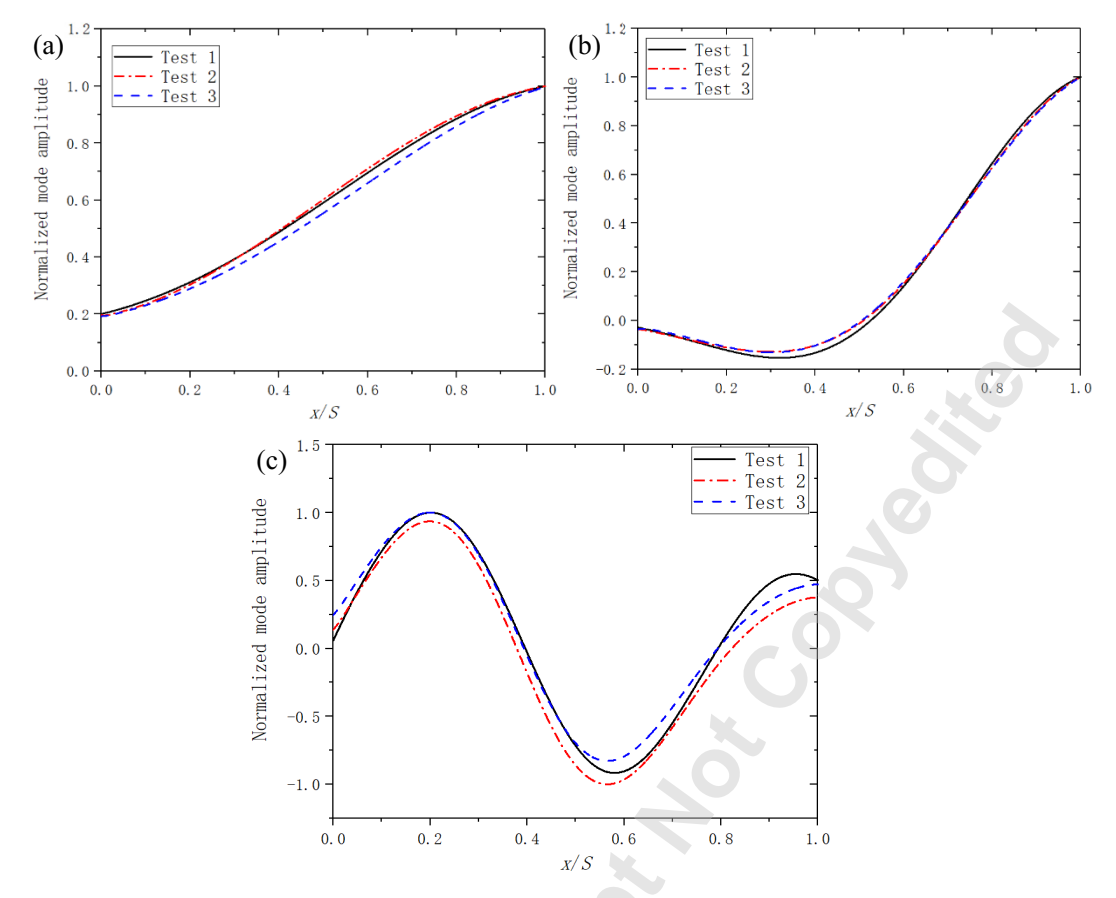


Fig. 8 (a) First, (b) second and (c) third normalized UMSs of the stationary fan blade obtained in the three tests.

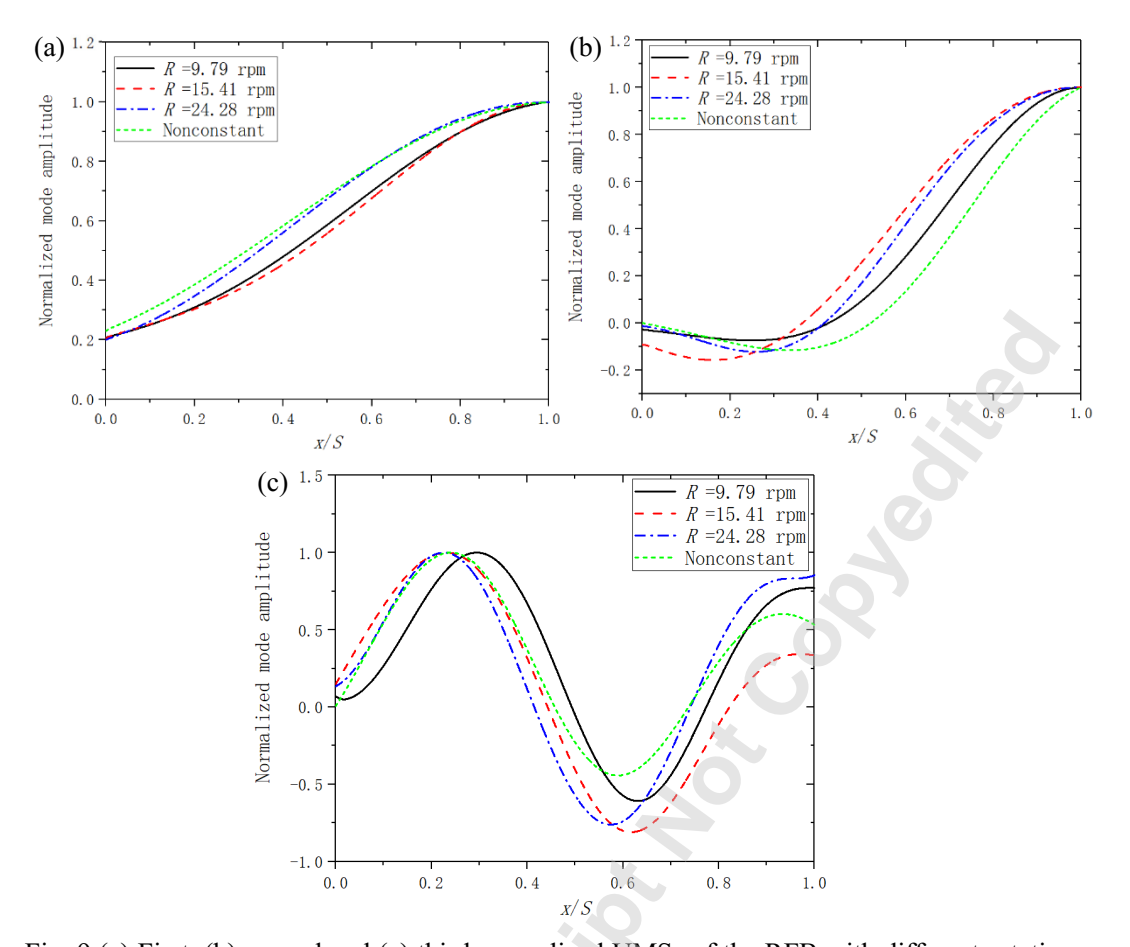


Fig. 9 (a) First, (b) second and (c) third normalized UMSs of the RFB with different rotation speeds.

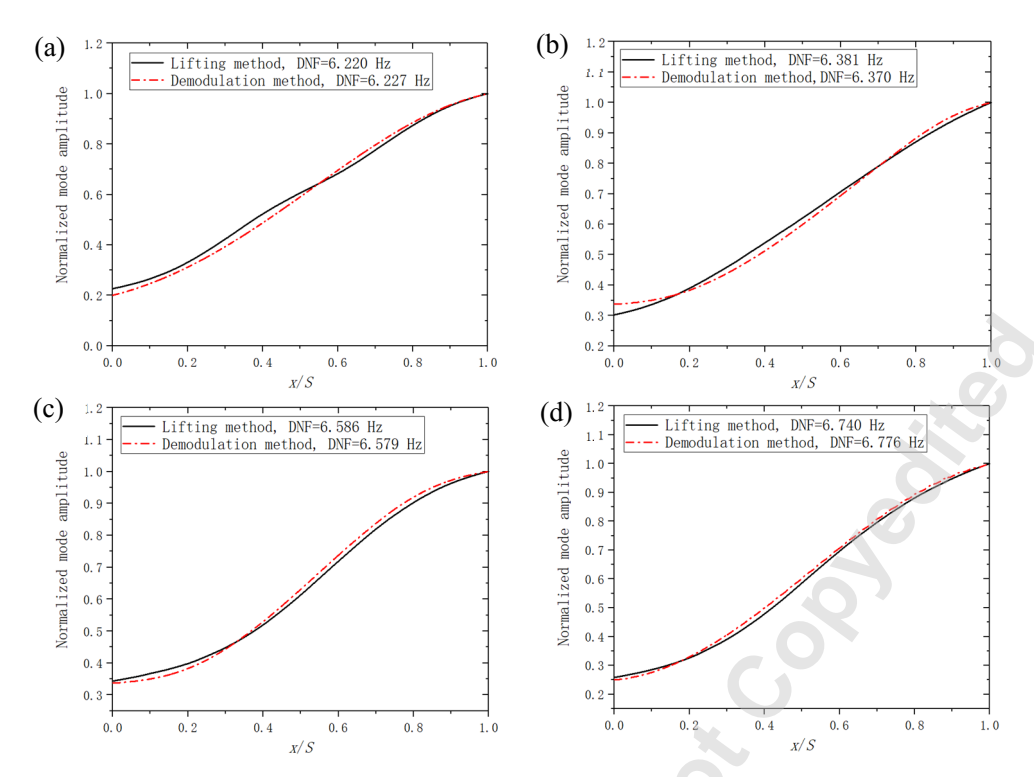


Fig. 10 First UMSs and DNFs of (a) the stationary fan blade, (b) the RFB with R = 10.9 rpm, (c) the RFB with R = 16.04 rpm, and (d) the RFB with R = 24.12 rpm estimated using the demodulation method and the lifting method in Ref. [32].

Zhu 39 VIB-21-1074